

H₂S SensorsDiorganotin Compounds Containing α -Aminoacidato Schiff Base Ligands Derived from Functionalized 2-Hydroxy-5-(aryldiazenyl)benzaldehyde. Syntheses, Structures and Sensing of Hydrogen SulfideTushar S. Basu Baul,^{*[a]} Anurag Chaurasiya,^[a] Monosh Rabha,^[a] Snehadrinarayan Khatua,^[a] Antonin Lyčka,^[b] Dieter Schollmeyer,^[c] and Klaus Jurkschat^{*[d]}

Abstract: Three novel bicycloazastannoxides, namely, $[n\text{Bu}_2\text{Sn}(\text{L}^1)]$ (**1**), $[n\text{Bu}_2\text{Sn}(\text{L}^2)]$ (**2**) and $[\text{Bz}_2\text{Sn}(\text{L}^3)]$ (**3**) were synthesized in one pot procedures by reacting diorganotin(IV) precursors with a mixture composed of an α -amino acid with either (*E*)-2-hydroxy-5-((4-nitrophenyl)diazenyl)benzaldehyde or (*E*)-2-hydroxy-5-(phenyldiazenyl)benzaldehyde. Single-crystal X-ray diffraction analysis reveal that compound **1** is monomeric, compound **2** consists of both a monomer and a dimer, while compound **3** is a coordination polymer for which two modifications **3A** and **3B** were identified. The ¹¹⁹Sn NMR chemical shifts

measured in CDCl₃ solutions indicate five-coordinate tin atoms for **1–3**. Further, compounds **1** and **2** were found to be highly selective for sensing hydrogen sulfide in UV/Vis channel in CH₃CN/H₂O (9:1) media. The development of orange red color is likely the results of a Brønsted-type acid-base reaction of H₂S with compounds **1** and **2**, respectively, giving di-*n*-butyltin sulfide and the corresponding pro-ligands H₂L¹ and H₂L², respectively. Theoretical calculations accompany the experimental work.

Introduction

The structurally vibrant organotin(IV) compounds have attracted immense interest in biological activity and catalysis.^[1,2] Among the organotin(IV) compounds, the use of carboxylate ligands provided a great variety of structures ranging from discrete mononuclear to polymeric complexes with the tin centers showing different coordination numbers. Apart from traditional

sustainable chemistry applications such as wood preservation to organic syntheses,^[2] carbon dioxide capture,^[3] homogeneous catalysts in PVC stabilization, polyurethane formation and transesterification,^[4] strong cytotoxic agents and diverse medicinal applications,^[1,5–9] organotin(IV) compounds have reached distinct heights as well. Strong Lewis acidity, rich molecular diversity and ease of synthesis led to the development of organotin-based molecular receptors for anions and ion pairs^[10] and others such as biomolecule functionalization, material applications and ternary mixed-valence metal clusters^[11–13] etc. to mention a few. On the other hand, the design and synthesis of multidentate bio-compatible amino acid derivatives with rich functional groups, possessing chirality and electronic asymmetry can offer fascinating properties and topologies when employed as building blocks for organotin(IV) compounds in supramolecular self-assembly, generating coordination polymers and multi-dimensional networks. Consequently, a variety of structurally characterized motifs based on diorganotin(IV) complexes of amino acetate Schiff bases were categorized viz., $[\text{R}_2\text{Sn}(\text{L})]$ (**I**), $[\text{R}_2\text{Sn}(\text{L})(\text{sol})]$ (**II**), $[\text{R}_2\text{Sn}(\text{L})_2]$ (**III**), $[\text{R}_2\text{Sn}(\text{L})\text{SnR}_2]$ (**IV**), $[\text{R}_2\text{Sn}(\text{L})(\text{sol})]_2$ (**V**), $[\text{R}_2\text{Sn}(\text{L})]_3$ (**VI**), and $[\text{R}_2\text{Sn}(\text{L})]_n$ (**VII**), where R = alkyl or aryl, L = variously substituted Schiff bases derived from α -amino acids and solv = donor solvent.^[14] Coordination modes in these complexes can vary from five to seven, thus providing access to a large variety of structural entities. Accordingly, these complexes demonstrated obvious exciting progress in various fields, such as cytotoxicity and

[a] Prof. Dr. T. S. Basu Baul, A. Chaurasiya, M. Rabha, Dr. S. Khatua
Centre for Advanced Studies in Chemistry, North-Eastern Hill University,
NEHU Permanent Campus, Umshing, Shillong 793 022, India
E-mail: basubaul@nehu.ac.in
basubaulchem@gmail.com

[b] Prof. Dr. A. Lyčka
Research Institute for Organic Syntheses (VUOS),
Rybitví 296, 533 54 Rybitví, Czech Republic

[c] Dr. D. Schollmeyer
Johannes Gutenberg-Universität Mainz, Institut für Organische Chemie,
Duesbergweg 10-14, 55099 Mainz, Germany

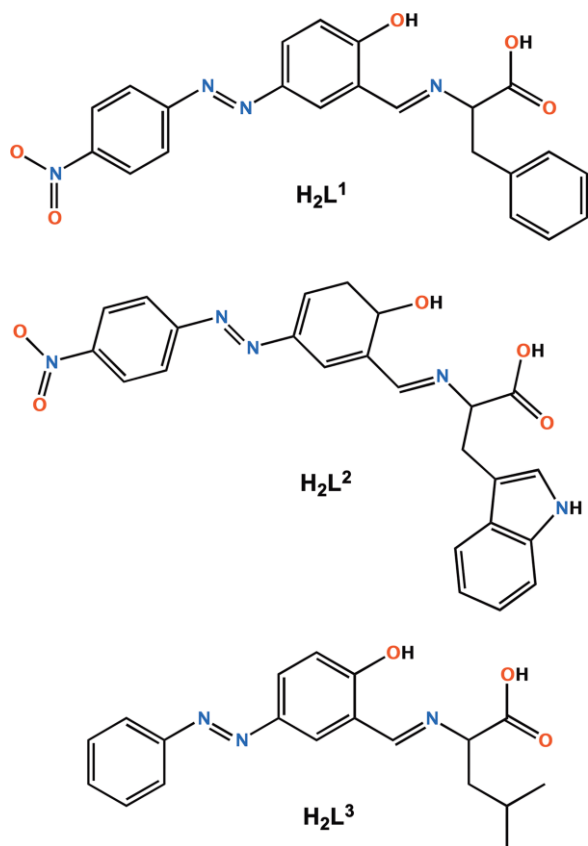
[d] Prof. Dr. K. Jurkschat
Technische Universität Dortmund, Fakultät für Chemie und Chemische
Biologie,
44221 Dortmund, Germany
E-mail: klaus.jurkschat@tu-dortmund.de

Supporting information and ORCID(s) from the author(s) for this article are available on the WWW under <https://doi.org/10.1002/ejic.202000177>.

© 2020 The Authors. Published by Wiley-VCH Verlag GmbH & Co. KGaA. This is an open access article under the terms of the Creative Commons Attribution License, which permits use, distribution and reproduction in any medium, provided the original work is properly cited.

antibacterial activity,^[15–20] photophysical properties useful for NLO applications,^[21] fluorescent staining of silk fibroin,^[19] and sensing^[22] as well as the detection of warfare agents (organophosphate based chemical weapons).^[23] These multifaceted applications of organotin(IV) compounds resulted mainly from their vast structural diversity.

During the course of writing this paper, a report describing the sensing ability of organotin(IV) compounds towards various metal ions such as Cu(II) and Fe(III) has appeared.^[24] However, to the best of our knowledge, sensing of hydrogen sulfide, H₂S, involving organotin(IV) compounds is hitherto unknown. The reasons for selecting H₂S as sensing agent are of utmost importance since it is the third most essential biological messenger (gasotransmitter) after NO and CO. H₂S plays a vital role in various physiological and pathological processes, such as vasodilatation, neuronal transmission, anti-oxidation, anti-apoptosis, insulin signaling and oxygen sensing etc.^[25] Inversely, the excessive level of H₂S causes various diseases such as stroke, Alzheimer's disease, cardiovascular disease, diabetes and liver cirrhosis.^[26] Recently, various colorimetric probes have been developed for highly selective and sensitive detection of H₂S. These probes are commonly based on H₂S-induced specific reactions, such as, reduction of azide to amine,^[27,28] thiolysis of dinitrophenyl ether^[29] and nucleophilic 1,4-addition^[30,31] and also metal sulfide precipitation.^[32,33] Consequently, ample studies on the development of advanced H₂S probe for rapid, sensitive and reliable detection techniques to know the physiological functions of H₂S is highly necessitated.



Scheme 1. Schematic drawing of the pro-ligands H₂L¹, H₂L², and H₂L³.

In previous studies we showed that the supramolecular structure in the solid state of Schiff base-containing diorganotin compounds can be controlled by using suitably functionalized 2-hydroxybenzaldehydes for the synthesis of the corresponding Schiff bases.^[14] This prompted us to explore the coordination chemistry of the deprotonated Schiff bases 2-((E)-{5-[(E)-(4-nitrophenyl)diazenyl]-2-oxidobenzylidene}amino)-3-phenylpropanoate, 3-(1*H*-indol-3-yl)-2-[(E)-{3-[(E)-(4-nitrophenyl)diazenyl]-6-oxidocyclohexa-1,3-dien-1-yl}methylene)amino]propanoate and 4-methyl-2-((E)-{2-oxido-5-[(E)-phenyldiazenyl]benzylidene}amino)pentanoate derived from the corresponding pro-ligands H₂L¹, H₂L², and H₂L³, respectively (Scheme 1).

Herein, we report the synthesis of three novel organotin compounds viz., [nBu₂Sn(L¹)] (**1**), [nBu₂Sn(L²)] (**2**) and [Bz₂Sn(L³)] (**3**), and characterize these by means of NMR spectroscopy, electrospray mass spectrometry, and single-crystal X-ray diffraction analyses. We also study their behavior towards H₂S.

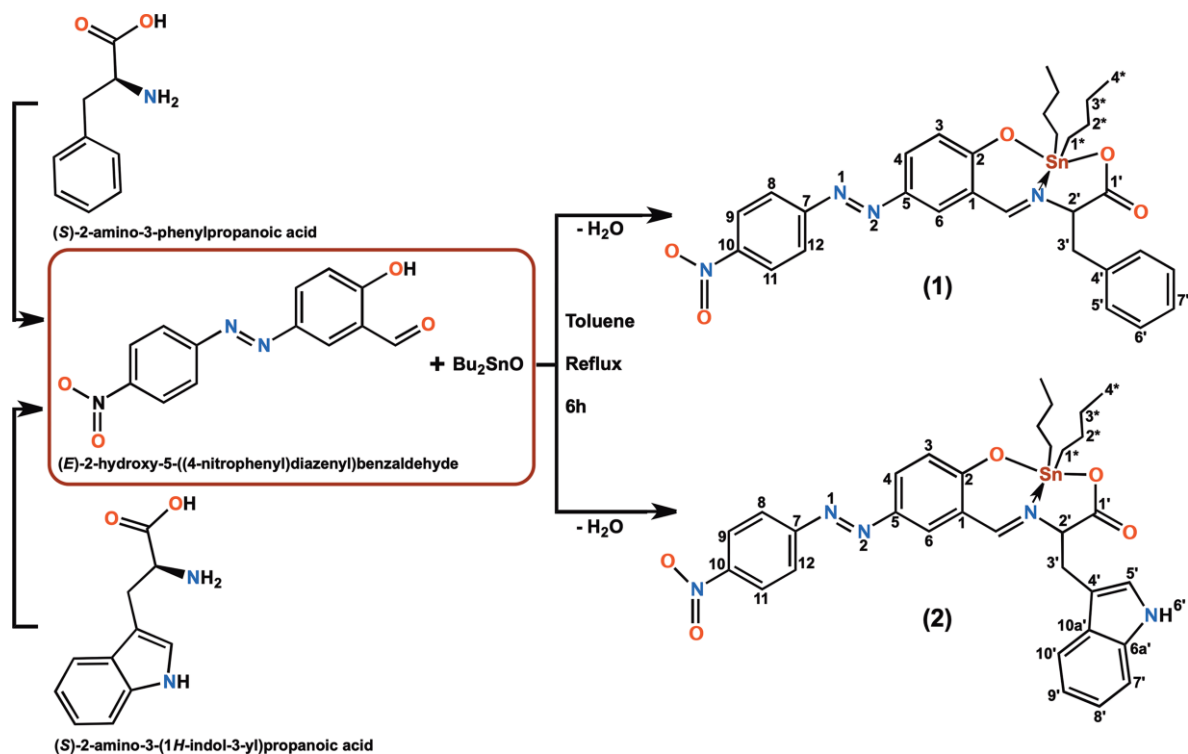
Results and Discussion

Synthesis and Characterization of 1–3

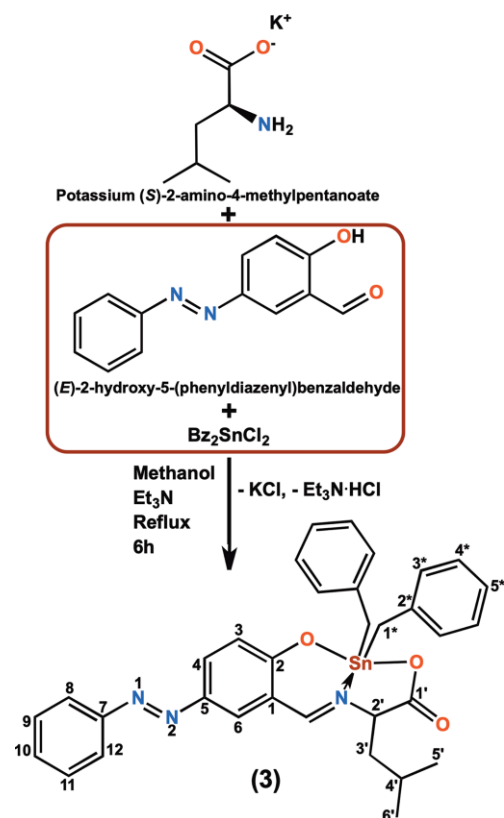
Compounds **1** and **2** were obtained from one-pot reactions between di-*n*-butyltin oxide, L-phenylalanine and (E)-2-hydroxy-5-[(4-nitrophenyl)diazenyl]benzaldehyde (for **1**), and di-*n*-butyltin oxide, (E)-2-hydroxy-5-(phenyldiazenyl)benzaldehyde and L-tryptophan (for **2**), respectively (Scheme 2).

In course of these reactions, the pro-ligands H₂L¹ and H₂L² were generated in situ from (E)-2-hydroxy-5-[(4-nitrophenyl)diazenyl]benzaldehyde and L-phenylalanine (for H₂L¹) or L-tryptophan (for H₂L²). Subsequently, these react with di-*n*-butyltin oxide giving compounds **1** and **2**, respectively. On the other hand, compound **3** was obtained, again in a one-pot reaction, from potassium leucinate, (E)-2-hydroxy-5-(phenyldiazenyl)benzaldehyde, and dibenzyltin dichloride, Bz₂SnCl₂ (Scheme 3). In course of this reaction, the pro-ligand KHL³ was formed which in turn reacted with Bz₂SnCl₂ and triethylamine, NEt₃, giving **3**. The concept of using one-pot multicomponent reaction avoids lengthy ligand preparation and characterization. The generation of the ligands was evident from the results collected from NMR spectroscopy and crystallography (vide infra). *Note: Attempts to prepare viable amount of the Schiff bases separately was not achieved owing to the insolubility of the amino acids in non-aqueous solvents and the possible formation of imine-zwitterionic species during the reactions.*

The compounds **1–3** were isolated in moderate yields upon successive recrystallization in a suitable solvent. The brown colored compounds are air-stable and possess good solubility in common organic solvents. IR spectroscopy revealed characteristic bands for the ν_{asym}(OCO), ν_{sym}(OCO) and ν(C=N) vibrations (see Experimental Section). The bonding mode of the carboxylate group was confirmed from the results of the single-crystal X-ray diffraction (SCXRD) analysis described below.



Scheme 2. Synthesis of the diorganotin compounds **1** and **2**. The atom numbering refers to the assignment of the ¹H and ¹³C NMR signals.



Scheme 3. Synthesis of the diorganotin compound **3**. The atom numbering refers to the assignment of the ¹H and ¹³C NMR signals.

Solid-State Molecular Structures of 1–3

Crystals suitable for single-crystal X-ray structure determination for **1–3** were obtained from ethanol by the slow solvent evaporation method. For compound **3**, two polymorphs were identified; **3A** (brown block) and **3B** (yellow needle) from the same batch of the crystalline material and both were investigated by SCXRD analysis (Table 1). Figure 1, Figure 2, and Figure 3 illus-

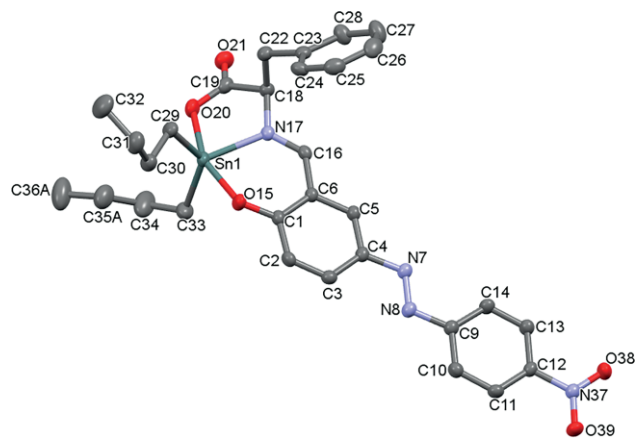


Figure 1. Displacement ellipsoid (50% probability level) plots of [nBu₂Sn(L¹)] (**1**) with partial atom labeling scheme. One of the butyl groups is disordered; only the main component is shown. Selected interatomic distances [Å]: Sn(1)–C(29) 2.123(4), Sn(1)–C(33) 2.119(4), Sn(1)–O(15) 2.107(2), Sn(1)–O(20) 2.161(3), Sn(1)–N(17) 2.169(3), C(16)–N(17) 1.297(4), C(18)–N(17) 1.469(4), C(19)–O(20) 1.296(4), C(19)–O(21) 1.213(4). Selected interatomic angles [°]: C(29)–Sn(1)–C(33) 131.32(16), C(29)–Sn(1)–N(17) 114.88(12), C(33)–Sn(1)–N(17) 113.80(14), O(15)–Sn(1)–O(20) 157.56(9).

Table 1. Crystal data, data collection parameters and convergence results for compounds **1**, **2**, and **3** (modifications **3A** and **3B**).

	1	2	3A	3B
Empirical formula	C ₃₀ H ₃₄ N ₄ O ₅ Sn	C ₆₄ H ₇₀ N ₁₀ O ₁₀ Sn ₂ , C ₃₂ H ₃₅ N ₅ O ₅ Sn	C ₃₃ H ₃₃ N ₃ O ₃ Sn	C ₃₃ H ₃₃ N ₃ O ₃ Sn
Formula weight	649.30	2065.01	638.34	638.34
Temperature/K	120	193	120	120
Crystal system	Monoclinic	Triclinic	Orthorhombic	Orthorhombic
Space group	<i>P</i> 2 ₁ / <i>c</i>	<i>P</i> $\bar{1}$	<i>P</i> 2 ₁ 2 ₁ 2 ₁	<i>P</i> na2 ₁
<i>a</i> /Å	9.1814(3)	13.5138(5)	9.4164 (2)	27.2350(12)
<i>b</i> /Å	29.2681(12)	17.8691(6)	11.1870(3)	9.5755(5)
<i>c</i> /Å	10.9610(4)	20.4456(7)	27.9969(9)	11.3148(5)
α /°	90	76.500(3)	90	90
β /°	98.769(3)	77.990(3)	90	90
γ /°	90	82.406(3)	90	90
<i>V</i> / Å ³	2911.03(19)	4677.5(3)	2949.23(15)	2950.8(3)
<i>Z</i>	4	2	4	4
ρ_{calcd} /cm ³	1.482	1.466	1.438	1.437
μ /mm ⁻¹	0.923	0.867	0.9	0.9
<i>F</i> (000)	1328	2112	1304	1304
Crystal size/mm ³	0.18 × 0.32 × 0.44	0.07 × 0.10 × 0.22	0.09 × 0.18 × 0.67	0.054 × 0.094 × 0.17
θ range for data collection/°	2.0 to 28.0	2.0 to 28.0	2.0 to 28.0	2.0 to 28.0
Index ranges	-12 ≤ <i>h</i> ≤ 12 -38 ≤ <i>k</i> ≤ 38 -14 ≤ <i>l</i> ≤ 11	-17 ≤ <i>h</i> ≤ 17 -23 ≤ <i>k</i> ≤ 23 -26 ≤ <i>l</i> ≤ 26	-11 ≤ <i>h</i> ≤ 12 -14 ≤ <i>k</i> ≤ 12 36 ≤ <i>l</i> ≤ 32	-35 ≤ <i>h</i> ≤ 30 -11 ≤ <i>k</i> ≤ 12 12 ≤ <i>l</i> ≤ 14
Reflections collected	16573	41931	12499	11133
Independent reflections [<i>R</i> _{int}]	6905 [0.0178]	22156 [0.043]	7018 [0.0202]	6465 [0.0443]
Data/restraints/parameters	6905/40/382	22156/0/1204	7018/0/363	6465/1/363
Goodness-of-fit on <i>F</i> ²	1.135	1.018	1.029	1.080
Final <i>R</i> indexes:				
<i>R</i> ₁ [<i>I</i> ≥ 2σ (<i>I</i>)]	0.0421	0.0509	0.0231	0.0592
w <i>R</i> ₂ [all data]	0.1056	0.1233	0.0554	0.1529
Largest diff. peak/hole /e Å ⁻³	2.47/ -1.59	0.88/ -0.9	0.34/ -0.43	0.94/ -1.86

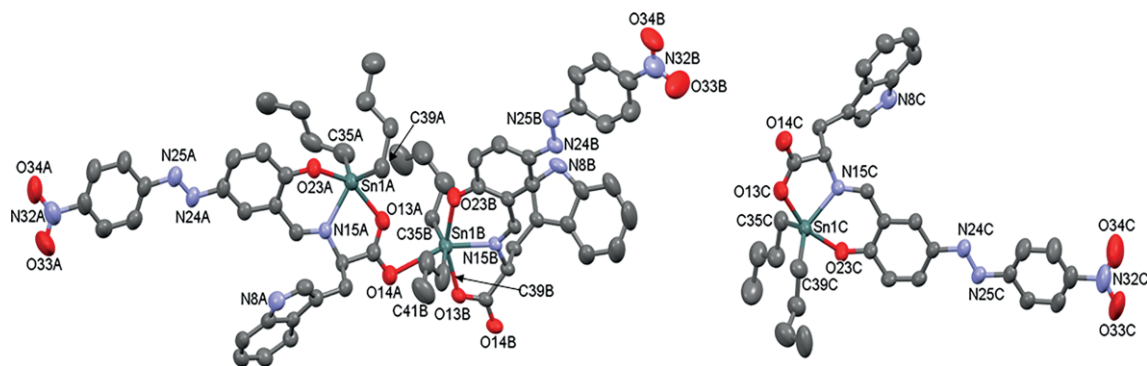


Figure 2. Displacement ellipsoid (50 % probability level) plots of $[n\text{Bu}_2\text{Sn}(\text{L}^2)]$ (**2**) with partial atom labeling scheme. Hydrogen atoms and C42B attached to C41B are omitted for clarity. The *n*-butyl groups C38A–C42A and C35B–C38B are disordered. Only major parts are shown. Also for clarity, the monomer (containing Sn1C) and the dimer (containing Sn1A and Sn1B) both present in the unit cell are shown separately. Figure S2 shows the precise arrangement of these two parts. Selected interatomic distances [Å]: Sn(1A)–C(35A) 2.125(6), Sn(1A)–C(39A) 2.123(5), Sn(1A)–O(13A) 2.184(3), Sn(1A)–O(23A) 2.079(3), Sn(1A)–N(15A) 2.175(3), Sn(1B)–C(35B) 2.122(5), Sn(1B)–C(39B) 2.160(6), Sn(1B)–O(13B) 2.206(3), Sn(1B)–O(23B) 2.143(3), Sn(1B)–N(15B) 2.218(3), Sn(1B)–O(14A) 2.717(3), Sn(1C)–C(35C) 2.116(5), Sn(1C)–C(39C) 2.147(5), Sn(1C)–O(13C) 2.145(3), Sn(1C)–O(23C) 2.096(3), Sn(1C)–N(15C) 2.164(3). Selected interatomic angles [°]: C(35A)–Sn(1A)–C(39A) 127.5(2), C(35A)–Sn(1A)–N(15A) 102.58(19), C(39A)–Sn(1A)–N(15A) 129.25(17), O(13A)–Sn(1A)–O(23A) 151.72(13), C(35B)–Sn(1B)–C(39B) 159.6(2), O(13B)–Sn(1B)–O(23B) 154.55(11), O(14A)–Sn(1B)–N(15B) 155.19(11), C(35C)–Sn(1C)–C(39C) 128.82(18), C(35C)–Sn(1C)–N(15C) 116.27(16), C(39C)–Sn(1C)–N(15C) 114.82(16), O(13C)–Sn(1C)–O(23C) 158.18(12).

trate the molecular structures of **1–3**, and the figure captions contain selected interatomic distances and angles.

Compound $[n\text{Bu}_2\text{Sn}(\text{L}^1)]$, **1**

The Sn(1) center in **1** is penta-coordinated and shows a distorted trigonal bipyramidal environment with the O(1) and O(2)

atoms occupying the axial and the N(17), C(29), and C(33) atoms occupying the equatorial positions. The distortion from the ideal trigonal bipyramidal geometry is especially evident from the O(15)–Sn(1)–O(20) angle of 157.56(9)° that considerably deviates from 180°. The Sn(1)–O(15) distance of 2.107(2) Å is shorter than the Sn(1)–O(20) distance of 2.161(3) Å. These

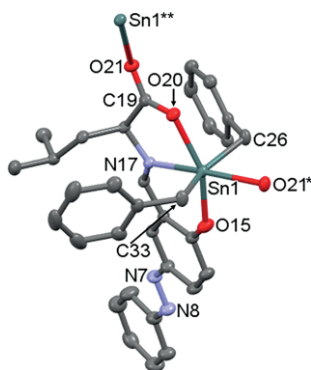


Figure 3. Displacement ellipsoid (50 % probability level) plots of $[Bz_2Sn(L^3)]_n$, **3A** with partial atom labeling scheme. Hydrogen atoms were omitted for clarity. Selected interatomic distances [Å]: Sn(1)–C(26) 2.142(3), Sn(1)–C(33) 2.127(3), Sn(1)–O(15) 2.092(2), Sn(1)–O(20) 2.227(2), Sn(1)–O(21) 2.449(2), Sn(1)–N(17) 2.236(3). Selected interatomic angles [°]: C(26)–Sn(1)–C(33) 151.57(12), O(15)–Sn(1)–O(20) 155.28(9), N(17)–Sn(1)–O(21) 172.91(9), Sn(1)–O(21)–C(19) 135.08(19). Symmetry code for O21*: $-x, -0.5 + y, 0.5 - z$. Symmetry code for Sn1**: $-x, 0.5 + y, 0.5 - z$.

distances are comparable to the values observed for structurally closely related dimethyl [2-((E)-[2-oxy-5-((E)-(4-nitrophenyl)diazenyl]benzylidene)amino)-3-phenylpropanoato]tin(IV) compound [Sn–O_{ph} 2.119(6) Å, Sn–O_{OCO} 2.146(6) Å] carrying tridentate ONO donor aminoacidato Schiff base ligand.^[14] The carboxylate moiety shows a monodentate coordination mode as the O(21) atom is not involved in any O→Sn interaction. The Sn(1)–N(17) distance of 2.169(3) Å reveals a strong N→Sn interaction. A similar Sn–N distance [2.151(7) Å] was reported for the related dimethyltin(IV) compound described above.^[14] In the crystal, compound **1** forms head-to-tail dimers via π – π interaction involving the phenyl moieties C(1)–C(6) and C(9)–C(14) at a centroid-to-centroid distance of 3.552(2) Å (Figure S1).

Compound $[nBu_2Sn(L^2)]_n$, **2**

The asymmetric unit in the crystal structure of **2** consists of three independent molecules corresponding to the metal centres Sn(1A), Sn(1B), and Sn(1C). Two of these molecules are connected into a dinuclear unit through an intermolecular O→Sn interaction. Similar to the Sn(1) center in compound **1**, the Sn(1A) and Sn(1C) centers are pentacoordinated and show slightly different distorted trigonal bipyramidal environments with C(35A), C(39A), N(15A) (at Sn1A) and C(35C), C(39C), N(15C) (at Sn1C) occupying the equatorial and O(13A), O(23A) (at Sn1A), and O(13C), O(23C) (at Sn1C) occupying the axial positions. The interatomic distances and angles involving the tin centers are similar to those of compound **1**. The O(13A)–Sn(1A)–O(23A) and O(13C)–Sn(1C)–O(23C) angles of 151.72(13) and 158.18(12) express the distortion from the ideal geometry. As a result of intermolecular O(14A)→Sn(1B) interaction at a distance of 2.717(3) Å, the Sn(1B) is hexacoordinated with a distorted octahedral environment. The distortion from the ideal geometry is reflected by the C(35B)–Sn(1B)–C(39B), O(13B)–Sn(1B)–O(23B), and O(14A)–Sn(1B)–N(15B) angles of 159.6(2), 154.55(11), and 155.19(11)°, respectively.

Compound $[Bz_2Sn(L^3)]_n$, **3**

Single crystals of compound **3** were obtained in two different modifications **3A** and **3B** with the orthorhombic space groups $P2_12_12_1$ and $Pna2_1$, respectively. The geometric parameters of these molecules differ only very little and consequently, only the structure of **3A** is discussed in detail (Figure 3, for **3B** see Figure S3). The Sn(1) center is hexacoordinated by C(26), C(33), O(15), O(20), O(21), and N(17) and shows a distorted octahedral environment with C(26)–Sn(1)–C(33), O(15)–Sn(1)–O(20), and N(17)–Sn(1)–O(21) angles of 151.57(12), 155.28(9), and 172.91(9)°, respectively. The Sn(1)–O(15) distance of 2.092(2) Å involving the phenolic oxygen atom is similar as compared to the corresponding distances in compounds **1** and **2**. The Sn(1)–O(20) distance of 2.227(2) Å involving the carboxylate oxygen atom is much longer. This is the result of the carboxylate moiety coordinating two tin atoms in a bridging mode. The Sn(1)–O(21) distance of 2.449(2) Å (that causes both modifications of compound **3** to be a one-dimensional coordination polymer, Figure S4) indicates a stronger intermolecular O→Sn interaction than observed for the dimer found in the structure of compound **2** [2.717(3) Å].

NMR Spectroscopic Characterization for **1–3**

The characterization of the diorganotin(IV) compounds **1–3** in solution was accomplished by means of their ¹H, ¹³C, ¹⁵N and ¹¹⁹Sn NMR spectra (see Figures S5–S22). The unambiguous assignment of ¹H and ¹³C chemical shifts was based on an appli-

Table 2. ¹H^[a] and ¹³C chemical shifts in compounds **1–3** in CDCl₃.^[b]

Proton/ Carbon No	1		2		3	
	¹ H	¹³ C	¹ H	¹³ C	¹ H	¹³ C
C(H)=N	7.70	172.3	7.43	171.7	7.82	171.9
1	–	116.3	–	116.3	–	116.5
2	–	171.1	–	173.1	–	172.4
3	6.84	123.7	6.85	123.8	6.88	123.1
4	8.06	128.9	8.05	128.9	8.11	130.1
5	–	143.8	–	143.6	–	143.8
6	7.57	135.9	7.39	135.6	7.54	132.9
7	–	155.7	–	155.7	–	152.4
8, 12	7.91	123.7	7.89	122.9	7.87	122.5
9, 11	8.32	124.6	8.32	124.7	7.52	129.1
10	–	148.0	–	148.1	7.44	130.6
1'	–	173.1	–	173.5	–	173.4
2'	4.29	69.9	4.33	69.0	3.63	66.3
3'	3.53, 3.09	41.7	3.81, 3.11	32.4	1.24, 0.65	44.3
4'	–	134.7	–	108.9	1.48	23.8
5'	7.12	130.1	6.94	124.6	0.82	22.5
6'	7.27	129.0	8.62	–	0.80	21.9
6a'	–	–	–	136.5	–	–
7'	7.27	127.6	7.62	118.6	–	–
8'	–	–	7.11	120.3	–	–
9'	–	–	7.21	122.8	–	–
10'	–	–	7.44	111.7	–	–
10a'	–	–	–	126.5	–	–

[a] Proton signals were overlapped in 1D ¹H NMR spectra and hence definitive multiplicity and coupling constants in aromatic part could not be assessed. [b] ¹H, ¹³C and ¹¹⁹Sn chemical shifts and ¹J(¹¹⁹Sn, ¹³C) coupling constants in di-*n*-butyltin(IV)- and dibenzyltin(IV) parts of compounds **1–3** in CDCl₃ are given in Table 3.

Table 3. ^1H , ^{13}C and ^{119}Sn chemical shifts and $^2J(^{119}\text{Sn}, ^1\text{H})$ and $^1J(^{119}\text{Sn}, ^{13}\text{C})$ coupling constants (in parentheses, Hz, ± 0.5 Hz) in di-*n*-butyltin(IV) and dibenzyltin(IV) parts of compounds **1–3** in CDCl_3 .

Compound	1* ^1H	^{13}C	2* ^1H	^{13}C	3* ^1H	^{13}C	4* ^1H	^{13}C	5* ^1H	^{13}C	^{119}Sn
1	1.37	22.1 (608.4)	1.67	26.8 [a]	1.37	26.5 (95.6)	0.93	13.4	–	–	–197.0
	1.40	22.0 (596.3)	1.49	26.7 [a]	1.25	26.3 (90.8)	0.79	13.3	–	–	–
2	1.39	22.3 (611.5)	1.67	26.9 [a]	1.39	26.6 (96.0)	0.94	13.5	–	–	–198.0
	1.42	22.1 (599.0)	1.50	26.8 [a]	1.26	26.4 (89.4)	0.81	13.4	–	–	–
3	3.11 + 3.05	29.5 (579.1)	–	136.7 (80.2)	7.26	128.2 (40.5)	7.21	128.8 (22.7)	7.08	125.6 (27.1)	–265.3
	2.89 + 2.84	29.8 (545.6)	–	136.4 (81.3)	6.90	122.5 (38.5)	6.93	128.5 (22.7)	6.99	125.2 (26.9)	–

[a] Not observed.

cation of standard 1D and selected 2D NMR experiments, viz., gradient-selected (gs)-correlation spectroscopy (COSY), total correlation spectroscopy (TOCSY), heteronuclear multiple-quantum correlation (HMQC), HMQC-RELAY, HMQC-TOCSY and heteronuclear multiple bond correlation (HMBC) allowing to assign all ^1H and ^{13}C resonances. Two sets of signals of equal intensities for the $n\text{Bu}_2\text{Sn}$ moieties in compounds **1** and **2** and for the Bz_2Sn moiety in compound **3** were observed because of diastereotopic environments following from an aliphatic stereogenic centre present in the ligand. Table 2 and Table 3 contain the ^1H and ^{13}C chemical shifts.

The gs-HMBC technique was used to determine ^1H - ^{15}N correlations with the experiment being optimized for coupling constants of 4 Hz, since $^3J(^{15}\text{N}, ^1\text{H})$ coupling constants are responsible for the formation of appropriate cross-peaks mainly in the $-\text{N}=\text{N}-$ fragment (Table 4). The expected number of ^{15}N resonances was observed in the gs-HMBC spectra. The ^{15}N chemical shifts of $\text{N}(\alpha)$, $\text{N}(\beta)$, $\text{C}(\text{H})=\text{N}$ and NO_2 are very similar in compounds **1–3**. The ^{119}Sn NMR spectra revealed sharp singlet resonances at $\delta = -197$ (**1**), $\delta = -198$ (**2**), and $\delta = -265$ ppm (**3**), respectively (Table 3). The ^{119}Sn chemical shifts indicate compounds **1** and **2** being monomeric with five-coordinate tin atoms.^[34] The same is valid for the dibenzyl derivative **3**.^[35] However, it cannot be excluded that each of the compounds **1–3** is involved in a monomer \rightleftharpoons dimer equilibrium which is fast on the ^{119}Sn NMR time scale and in which the monomer dominates under the experimental conditions (given concentration, room temperature) used for the measurement. However, this equilibrium was not investigated in more detail.

Table 4. ^{15}N chemical shifts in compounds **1–3** in CDCl_3 .

Nitrogen No.	1	2	3
N1 (α)	100.1	99.5	99.5
N2 (β)	129.7	129.2	115.1
$\text{C}(\text{H})=\text{N}$	–165.3	–165.1	–161.1
NO_2	–12.4	–12.6	–
NH	–	–256.1	–
$^1J(^{15}\text{N}, ^1\text{H})$ [Hz]	–	98.6	–

The following equation^[36] was proposed for the estimation of C–Sn–C angles in di-*n*-butyltin derivatives using absolute values of the $^1J(^{119}\text{Sn}, ^{13}\text{C})$ coupling constants:

$$|^1J(^{119}\text{Sn}, ^{13}\text{C})| = (9.99 \pm 0.73) \theta - (746 \pm 100)$$

$$(r = 0.982; n = 9)$$

Based on the two $^1J(^{13}\text{C}-^{119}\text{Sn})$ coupling constants (608.4 and 596.3 Hz for **1**; 611.5 and 599.0 Hz for **2**), the calculated angles θ are 135.6° and 134.4° (for **1**), and 135.9° and 134.6° (for **2**), respectively.

Colorimetric Detection of Hydrogen Sulfide (H_2S)

The compounds **1** and **2** are both faint yellow colored in aqueous CH_3CN solution ($\text{CH}_3\text{CN}:\text{H}_2\text{O}$; 9:1, v/v), and they absorb at 386 nm and 381 nm, respectively. Firstly, the anion selectivities of compounds **1** and **2** were evaluated by measuring their colorimetric responses toward various anions (F^- , Cl^- , Br^- , I^- , AcO^- , CN^- , NO_3^- , OH^- , H_2PO_4^- and HSO_4^-) in aqueous CH_3CN solution. As shown in Figure 4a, the appearance of a new band at 450 nm accompanied by a significant development of orange red color is observed only in the presence of 5 equiv. of H_2S (using NaHS as source of H_2S), while other anions do not show any color change. During the absorbance titration of **1** with increasing amount of H_2S (0–5.0 equiv.), the absorbance at 386 nm is gradually decreased and a band at 450 nm is increased gradually with a red shift of 64 nm in aqueous CH_3CN solution (Figure 4b). No further enhancement of absorption was observed even after the addition of more than 5.0 molar equiv. of H_2S , which confirms the completion of the reaction (Figure 4c). The linear enhancement of absorbance ratio at 450 nm and 386 nm (A_{450}/A_{386}) with lower H_2S concentration (0–25 μM) potentially allows H_2S quantification. In analogy to **1**, compound **2** also shows H_2S selectivity under similar condition, the mixture of compound **2** and H_2S absorbs at 455 nm and a red shift of 64 nm was observed (Figure 5a and 5b). The plot of A_{455}/A_{384} vs. H_2S concentration shows linear enhancement of absorbance ratio with lower H_2S concentration (0–25 μM) as observed for compound **1** (Figure 5c). It is noteworthy that under similar conditions, compound **3** did not show selectivity to

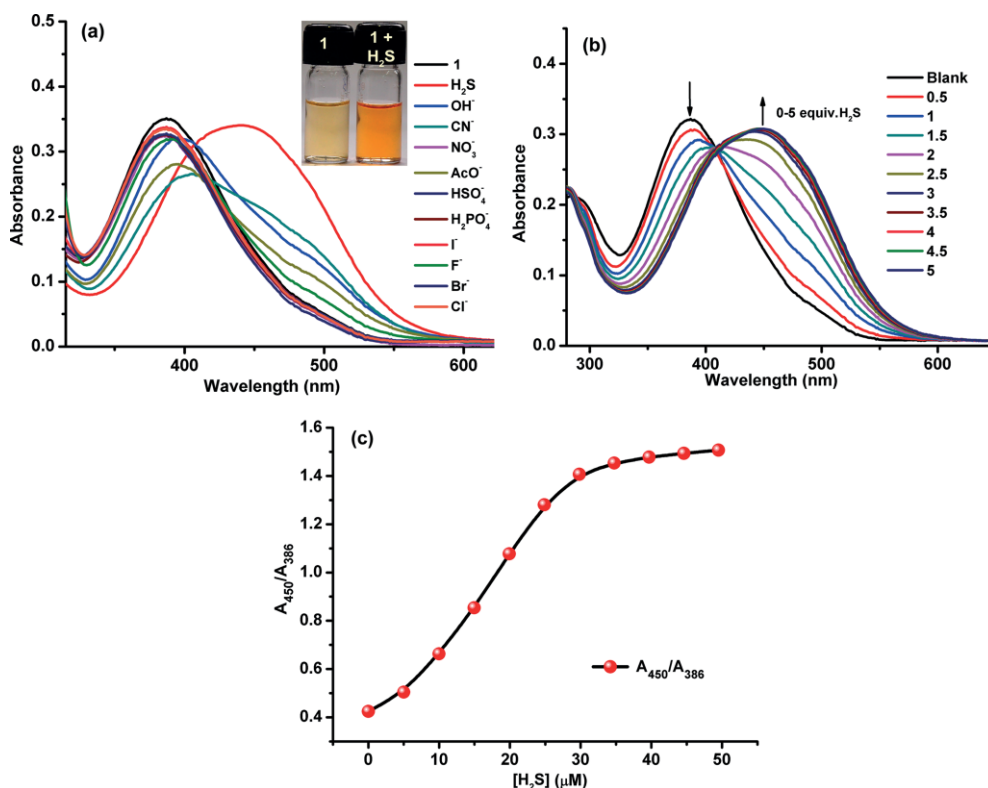


Figure 4. (a) UV/Vis spectra of an aqueous CH₃CN solution of **1** (10 μM) to which various anions (50 μM) had been added. (Inset) Digital photograph of **1** and **1** + H₂S solutions under ambient light showing color change. (b) Absorption titration of **1** (10 μM) in CH₃CN/H₂O (9:1; v/v) with increasing amount of H₂S solution (0–50 μM). (c) Plot of absorbance ratio (A_{450}/A_{386}) at 450 nm and 386 nm vs. concentration of H₂S.

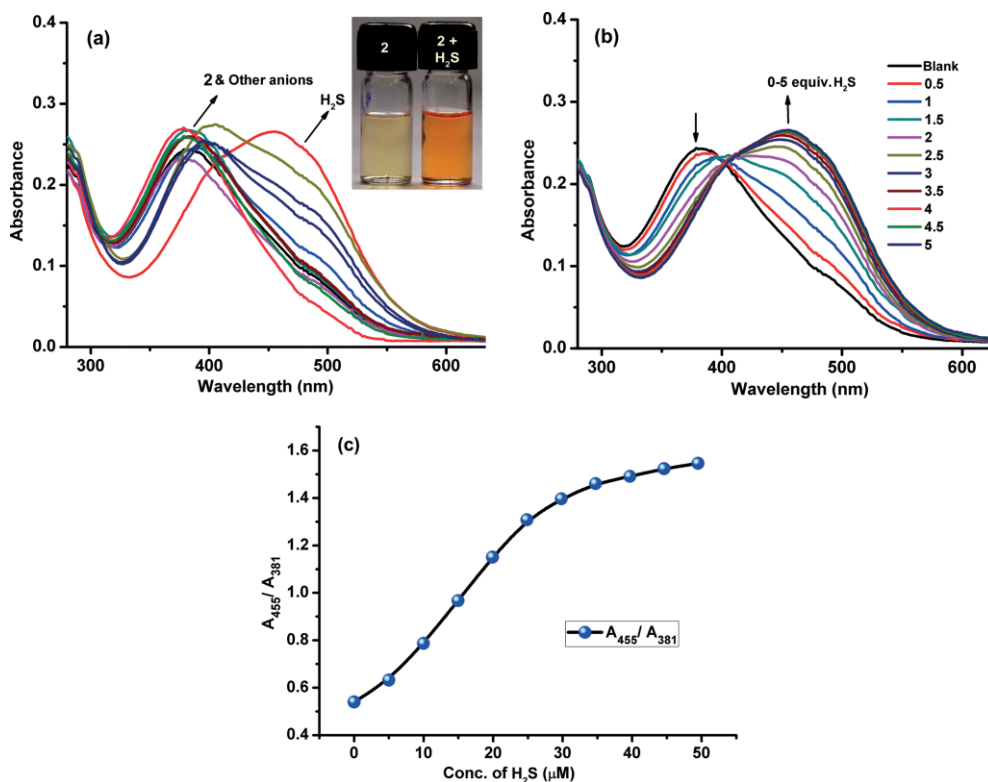


Figure 5. (a) UV/Vis spectra of an aqueous CH₃CN solution of **2** (10 μM) to which various anions (50 μM) had been added. (Inset) Digital photograph of **2** and **2** + H₂S solutions under ambient light showing color change. (b) Absorption titration of **2** (10 μM) in CH₃CN/H₂O (9:1; v/v) with increasing amount of H₂S solution (0–50 μM). (c) Plot of absorbance ratio (A_{455}/A_{381}) at 455 nm and 381 nm vs. concentration of H₂S.

any analyte of our interest (vide supra) (Figure 6). We have no explanation for this behavior.

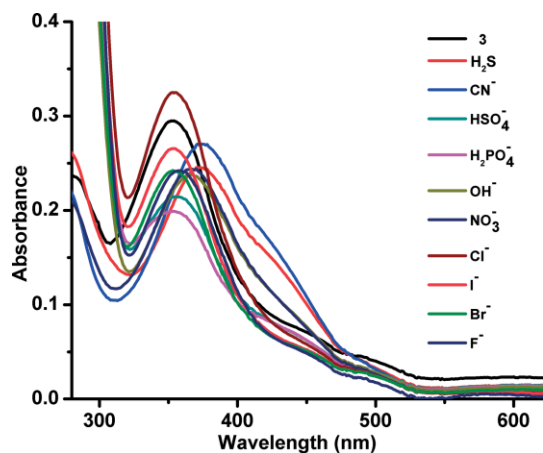
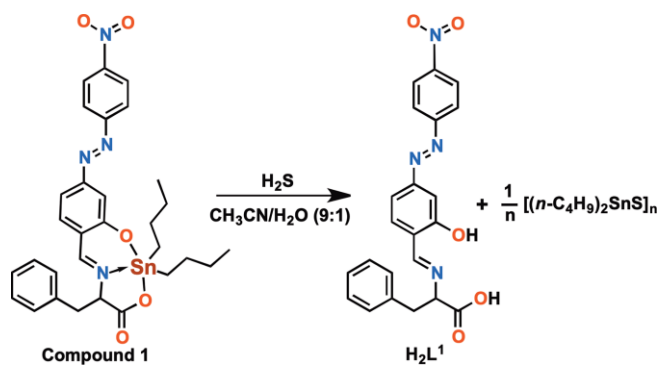


Figure 6. UV/Vis spectra of a solution of **3** (10 μM) in CH₃CN:H₂O (9:1; v/v) to which various anions (50 μM) had been added.

Monitoring the Reaction between Compound **1** and H₂S by Means of NMR Spectroscopy and Mass Spectrometry

To verify the mode of reactions of H₂S with **1** and **2**, and to find the reasons for color change, the following methodology was adopted. Firstly, **1** was mixed with NaHS (5 equiv.; Source of H₂S) in methanol/water (9:1) and the ESI-mass spectrum was recorded (Figure S23). The ESI-MS spectrum displayed a mass cluster centered at *m/z* 419.135 (calcd. *m/z* 419.140) corresponding to [C₂₂H₁₈N₄O₅ + H]⁺, and confirming the formation of the pro-ligand H₂L¹. In view of these information, a plausible Scheme 4 has been suggested where the formations of di-*n*-butyltin sulfide [(*n*-C₄H₉)₂SnS]_{*n*} and the corresponding H₂L¹ has been suggested. This was further verified by ¹H NMR titrations (Figure 7).



Scheme 4. Reaction of **1** with H₂S showing the formation of H₂L¹ and di-*n*-butyltin sulfide [(*n*-C₄H₉)₂SnS]_{*n*}.

¹H NMR spectrum of compound **1** in [D₆]DMSO displays six sets of proton signals in the aromatic region. During the ¹H NMR titration with H₂S (0–7 equiv.) in [D₆]DMSO/D₂O (9:1) mixture, all the proton signals shifted downfield which is expected to be the signals arising from the H₂L¹ skeleton. To verify this, ¹H NMR spectra of (*E*)-2-hydroxy-5-[(4-nitrophenyl)diazenyl]benzaldehyde, a mixture consisting of (*E*)-2-hydroxy-5-[(4-nitro-

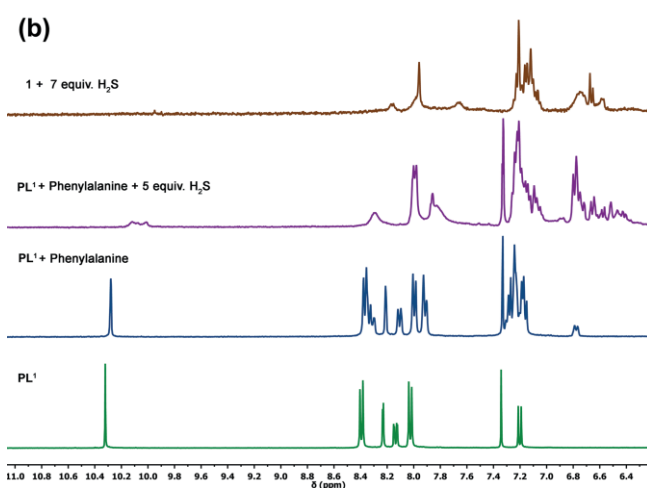
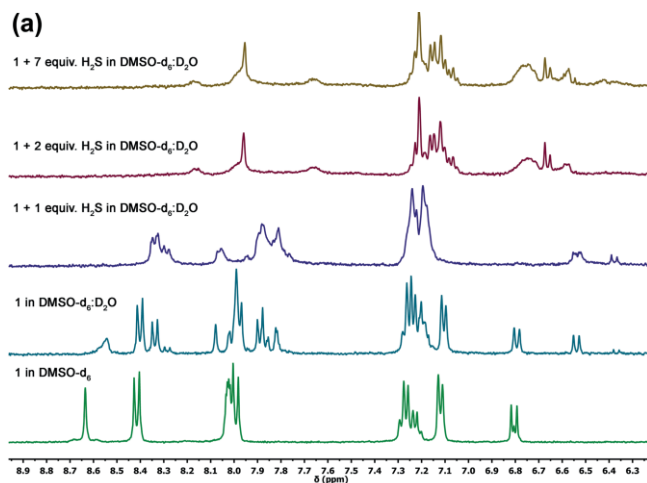


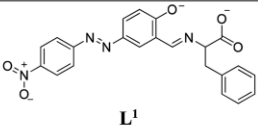
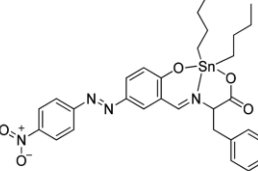
Figure 7. Parts of ¹H NMR spectra of (a) compound **1** to which various amounts of H₂S had been added, and (b) (*E*)-2-hydroxy-5-[(4-nitrophenyl)diazenyl]benzaldehyde, a mixture of (*E*)-2-hydroxy-5-[(4-nitrophenyl)diazenyl]benzaldehyde and phenylalanine, and a mixture of (*E*)-2-hydroxy-5-[(4-nitrophenyl)diazenyl]benzaldehyde, phenylalanine with 5 equiv. of H₂S in [D₆]DMSO/D₂O (9:1).

phenyl)diazenyl]benzaldehyde and phenylalanine (1:1), and the mixture consisting of (*E*)-2-hydroxy-5-[(4-nitrophenyl)diazenyl]benzaldehyde, phenylalanine (1:1) and H₂S (5 equiv.) were recorded and compared. The ¹H NMR spectrum of the latter mixture is found to be very similar to the spectrum that is observed for **1** + H₂S (1:7) mixture. This result clearly supports the formation of the ligand H₂L¹ as a result of the reaction between **1** and H₂S.

DFT Calculations

Time dependent-density functional theory (TD-DFT) calculations were performed to obtain insight into the electronic transitions responsible for the absorption spectra of compound **1** and deprotonated ligand L¹. The calculated vertical excitation energies, corresponding oscillator strength (*f*) and composition of the related transitions assigned to the experimental UV/Vis spectrum in CH₃CN are collected in Table 5. The TD-DFT calculation indicates that the experimentally obtained spin allowed

Table 5. Calculated (selective) and experimentally obtained optical transitions for L¹ and compound **1**.

Compounds	Experimentally observed emission energy [eV(nm)]	Computed vertical excitation transition [eV(nm)]	<i>f</i> ^[a]	Transitions	CI ^[b]
 L ¹	2.76 eV (450 nm)	2.74 eV (452 nm)	0.028	HOMO-5→LUMO	0.46
 Compound 1	3.21 eV (386 nm)	3.27 eV (379 nm)	0.075	HOMO→LUMO+1	0.69

[a] *f* = oscillator strength. [b] CI = coefficients are in absolute values.

π - π^* transition band at $\lambda_{\max} = 386$ nm (3.21 eV) is due to the strong transitions from HOMO→LUMO+1 ($f = 0.075$) (379 nm, 3.27 eV) (Figure 8). After reaction with H₂S, the compound **1** releases the pro-ligand (H₂L¹), which absorbs strongly at 450 nm generating orange red color. The orange red color could be due to the spin allowed transition from HOMO-5→LUMO ($f = 0.028$) (452 nm, 2.74 eV) (Figure 8). Thus, the TD-DFT results evidently support the hypothesis that H₂S senses by changing the color to orange red owing to the generation of H₂L¹.

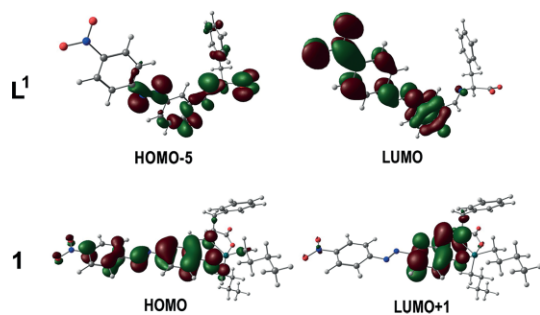


Figure 8. Views of the frontier molecular orbitals (MOs) of L¹ and compound **1** obtained from TD-DFT calculation [isovalue = 0.03].

Conclusions

Simple and time-saving three-component one-pot reactions were used for the syntheses of three novel intramolecularly coordinated diorganotin compounds. Slight variations of the in situ-formed ligand backbones on the one hand and variation of the organic substituents at the tin center (*n*-butyl vs. benzyl) caused different structures in the solid state. These ranged from monomers with a pentacoordinated tin center in **1** via a combination of a coordination dimer and a monomer with both penta- and hexacoordinated tin centers in **2** to a coordination polymer with hexacoordinated tin centers in **3**. Most importantly, compounds **1** and **2** react with H₂S in a Brønsted-type acid-base reaction giving (*n*Bu₂SnS)_{*n*} and the corresponding pro-ligands H₂L¹ and H₂L², respectively. The reactions are ac-

companied with a color change and enable easy detection of H₂S. The general concept of using organometallic compounds for the detection of Brønsted acids holds great potential for future work. Tailor-made systems can be designed by comparing the p*K*_a values of the pro-ligands (H₂L) the anion of which is bound to the metal centers (giving ML) with the p*K*_a value of the Brønsted acid HL' (or H₂L') to be detected. The p*K*_a value of HL' (or H₂L') should be lower than the p*K*_a value of H₂L, and H₂L should have a different color than ML.

Experimental Section

Materials and Physical Measurements

Reagents such as 4-nitroaniline, 2-hydroxybenzaldehyde, L-leucine, L-phenylalanine, L-tryptophan (Spectrochem) and di-*n*-butyltin oxide (Fluka) were used without further purification, while aniline (SD Fine) was freshly distilled prior to use. All anionic salts used for sensing studies were purchased from commercial suppliers (Aldrich, Alfa Aesar, and Spectrochem) and were used as received without further purification. The solvents used in the reactions were of AR grade and dried using standard procedures. Toluene and hexane were distilled from benzophenone/sodium, whereas methanol and dichloromethane were distilled from activated magnesium and calcium hydride, respectively. Dibenzyltin dichloride was prepared by following the literature method.^[37] Melting points were measured using a Büchi M-560 melting point apparatus and are uncorrected. Elemental analyses were performed using a Perkin Elmer 2400 series II instrument. IR spectra in the range 4000–400 cm⁻¹ were obtained on a Perkin Elmer Spectrum BX series FT-IR spectrophotometer with samples investigated as KBr discs (Figure S24–S28). ¹H, ¹³C, ¹⁵N and (¹¹⁹Sn NMR spectra in the case of compounds **1–3**) were recorded on a Bruker Avance III HD 400 spectrometer and measured at 400.13 MHz, 100.62 MHz, 40.55 MHz and 149.12 MHz, respectively, in CDCl₃ using a 5 mm tunable PRODIGY cryo probe. The ¹H and ¹³C chemical shifts were referenced to internal Me₄Si ($\delta = 0.00$ ppm), while ¹⁵N and ¹¹⁹Sn chemical shifts were referenced to external neat CH₃NO₂ and external neat Me₄Sn, respectively, in a co-axial capillary ($\delta = 0.00$ ppm). The ¹¹⁹Sn NMR spectra of compounds **1–3** in CDCl₃ solution were measured using inverse-gated decoupling. All 2D experiments, viz., COSY, TOCSY, HMQC, HMQC-RELAY, HMQC-TOCSY and HMBC were performed using manufac-

turer's software (TOPSPIN 3.5). NMR and IR spectra are appended in Figures S5–S22 and Figures S24–S28, respectively.

For sensing studies, ^1H NMR titrations were carried out on a Bruker AVANCE II 400 spectrometer and chemical shifts were expressed in ppm using the residual protic solvent resonance as the internal standard. UV/Visible spectra were recorded on an Agilent Cary 60 UV/Vis spectrophotometer with a quartz cuvette (path length = 1 cm). All spectroscopic measurements were performed in organic solvent (CH_3CN) and Millipore water. Stock solutions (1 mM) of compounds **1–3** were prepared in CH_3CN and diluted to 10 μM using millipore water ($\text{CH}_3\text{CN}/\text{H}_2\text{O}$; 9:1; v/v) for UV/Vis spectroscopic studies. Stock solutions (10 mM) of various anions were prepared using their tetra-*n*-butylammonium or sodium salts in Millipore water.

Full geometry optimizations of compound **1** and ligand L^1 (refer to Introduction for the abbreviation) were carried out using DFT method with the Gaussian 09 program package in the ground states. The B3LYP/6-31G (d,p)^[38] basis set was assigned for all elements. Time dependent density functional (TD-DFT) calculations, using the polarizable continuum model (PCM)^[39] non-equilibrium version, were performed with a spin-restricted formalism to examine low-energy excitations at the ground-state geometry in CH_3CN at the same level of calculation as employed for geometry optimizations.

Synthesis of (E)-2-Hydroxy-5-[(4-nitrophenyl)diazanyl]benzaldehyde and (E)-2-Hydroxy-5-(phenyldiazanyl)benzaldehyde: These compounds were prepared by reacting the appropriate aryl-diazonium chloride with 2-hydroxybenzaldehyde, following previously reported procedures^[14,40,41] and the purities were established by their physical and spectroscopic characterization prior to use.

Synthesis of Di-*n*-butyltin(IV) Compounds **1 and **2**:** The di-*n*-butyltin(IV) compounds **1** and **2** (Scheme 1) were prepared following one pot reaction by the same synthetic route and, hence, only the general procedure is outlined here. A 100 mL three necked round-bottomed flask was charged with a mixture of the amino acid (L-phenylalanine or L-tryptophan) (0.60 mmol), (E)-2-hydroxy-5-[(4-nitrophenyl)diazanyl]benzaldehyde (0.60 mmol), and di-*n*-butyltin(IV) oxide (0.60 mmol), fitted with a Dean–Stark moisture trap and a water-cooled condenser. After addition of anhydrous toluene (50 mL) whilst stirring, the suspension was heated to reflux for around 1 h. After that time, complete dissolution of the reactants was accomplished giving a clear solution in both cases. The mixture was heated at refluxed for additional 5 h to ensure reaction completion, and filtered while hot. Then, the filtrate was evaporated to dryness using a rotary evaporator and the residue was dried in vacuo. The solid mass was extracted into a minimum amount of benzene and precipitated with hexane and this process was repeated thrice. After filtration, the residue was dried in vacuo which afforded brown powder.

Compound 1: The initial reaction product was recrystallized from ethanol to give brown microcrystalline product of **1**. Yield: 0.30 g, 76 %. M.p.: 164–165 °C. Anal. calcd. (%) for $\text{C}_{30}\text{H}_{34}\text{N}_4\text{O}_5\text{Sn}$: C 55.49, H 5.28, N 8.63; found C 55.89, H 5.38, N 8.60. IR absorption (cm^{-1}): 1689 $\nu_{\text{asym}}(\text{OCO})$, 1614 $\nu(\text{C}=\text{N})$, 1524, 1469, 1390, 1340, 1197, 1159, 1145, 1113, 1105, 854, 697, 604.

Compound 2: The initial reaction product was recrystallized from ethanol to give brown microcrystalline product of **2**. Yield: 0.35 g, 84 %. M.p.: 170–171 °C. Anal. calcd. (%) for $\text{C}_{96}\text{H}_{105}\text{N}_{15}\text{O}_{15}\text{Sn}_3$: C 55.83, H 5.12, N 10.17; found C 55.77, H 5.20, N 10.50. IR absorption (cm^{-1}): 3435 $\nu(\text{NH})$, 1667 $\nu_{\text{asym}}(\text{OCO})$, 1615 $\nu(\text{C}=\text{N})$, 1520, 1469, 1385, 1340, 1253, 1193, 1143, 1106, 854, 749, 604.

Compound 3: A methanol solution (20 mL) of potassium hydroxide (0.043 g, 0.752 mmol) was added dropwise to a stirred suspension of L-leucine (0.1 g, 0.752 mmol) containing 20 mL of methanol and the clear solution was filtered in a 100 mL round-bottomed flask. To this clear solution, a methanol solution (20 mL) of (E)-2-hydroxy-5-(phenyldiazanyl)benzaldehyde (0.17 g, 0.752 mmol) and methanol solution (5 mL) of Bz_2SnCl_2 (0.28 g, 0.752 mmol) were added successively whilst stirring conditions. The reaction mixture remained clear for about half an hour and triethylamine (0.08 g, 0.752 mmol) was added and then the reaction mixture was heated to reflux for 6 hours. The reaction mixture was filtered while hot and the solvent was removed using rotary evaporator and dried in vacuo giving a solid residue. The latter was extracted in anhydrous benzene and purified by precipitating with hexane and the process of precipitation was repeated thrice. The crude product was crystallized using ethanol, which upon slow evaporation afforded yellowish brown microcrystalline material. Yield: 0.30 g, 62 %. M.p.: 175–176 °C. Anal. calcd. (%) for $\text{C}_{33}\text{H}_{33}\text{N}_3\text{O}_3\text{Sn}$: C 62.09, H 5.21, N 6.58; found C 61.89, H 5.44, N 7.42. IR absorption (cm^{-1}): 1618 $\nu_{\text{asym}}(\text{OCO})$, 1607 $\nu(\text{C}=\text{N})$, 1533, 1473, 1377, 1194, 1135, 1110, 767, 755, 699, 595, 499.

X-ray crystallography

Intensity data for compounds **1–3** were collected at low temperature with Mo- K_{α} radiation ($\lambda = 0.71073 \text{ \AA}$) on a STOE IPDS 2T diffractometer with image plate detector. The data were processed using the standard STOE software. All structures were solved using SIR-2004 (direct methods) and were refined with SHELXL-2018. For further details see Table 1.

CCDC 1936179 (for **1**), 1936180 (for **2**), 1936181 (for **3A**), and 1936182 (for **3B**) contain the supplementary crystallographic data for this paper. These data can be obtained free of charge from The Cambridge Crystallographic Data Centre.

Conflict of Interest

The authors declare that they have no conflicts of interest with the contents of this article.

Supporting Information (see footnote on the first page of this article): Views of the crystal structures of compounds **1** and **3** (Figures S1–S4), ^1H , ^{13}C , ^{15}N and ^{119}Sn NMR spectra (Figures S5–S22), ESI-MS (Figure S23) and IR spectra (Figures S24–28).

Acknowledgments

This research received financial support from the Department of Biotechnology, India (Grant No. BT/PR 25263/NER/95/1104/2017, TSBB) and DST SERB (SB/FT/CS/115/2012). TSBB and SK thank Bhaskar Sen, NEHU for theoretical calculations. Open access funding enabled and organized by Projekt DEAL.

Keywords: Tin · Ligands with azo-imino groups · Structure elucidation · Sensing studies

- [1] M. Gielen, E. R. T. Tiekink, *50Sn Tin Compounds and Their Therapeutic Potential, in Metallotherapeutic Drug and Metal-Based Diagnostic Agents* (Eds.: M. Gielen, E. R. T. Tiekink), John Wiley & Sons Ltd, Chichester, England **2005**, Ch. 22, pp. 421–439, and references cited therein.
- [2] A. G. Davies, M. Gielen, K. H. Pannell, E. R. T. Tiekink (Eds.), *Tin Chemistry - Fundamentals, Frontiers and Applications*, John Wiley & Sons Ltd, Chichester, England **2008**.
- [3] L. Plasseraud, D. Ballivet-Tkatchenko, H. Cattey, S. Chambrey, R. Ligabue, P. Richard, R. Willem, M. Biesemans, *J. Organomet. Chem.* **2010**, 695, 1618–1626.

- [4] E. Arkis, *Organotin Compounds as PVC stabilizers, in Tin Chemistry - Fundamentals, Frontiers and Applications* (Eds.: A. G. Davies, M. Gielen, K. H. Pannell, E. R. T. Tiekink), John Wiley & Sons Ltd, Chichester, England **2008**, Ch. 3.3, pp. 312–323, and references cited therein.
- [5] M. K. Amir, S. Khan, Zia-ur-Rehman, A. Shah, I. S. Butler, *Inorg. Chim. Acta* **2014**, *423*, 14–25.
- [6] F. Arjmand, S. Parveen, S. Tabassum, C. Pettinari, *Inorg. Chim. Acta* **2014**, *423*, 26–37.
- [7] C. E. Carraher Jr., M. R. Roner, *J. Organomet. Chem.* **2014**, *751*, 67–82.
- [8] L. Niu, Y. Li, Q. Li, *Inorg. Chim. Acta* **2014**, *423*, 2–13.
- [9] M. Z. Bulatović, D. Maksimović-Ivanić, C. Bensing, S. Gómez-Ruiz, D. Steinborn, H. Schmidt, M. Mojić, A. Korać, I. Golić, D. Pérez-Quintanilla, M. Momčilović, S. Mijatović, G. N. Kaluđerović, *Angew. Chem. Int. Ed.* **2014**, *53*, 5982–5987; *Angew. Chem.* **2014**, *126*, 6092.
- [10] M. M. Naseer, K. Jurkschat, *Chem. Commun.* **2017**, *53*, 8122–8135.
- [11] J.-P. Berndt, A. Engel, R. Hrdina, S. Dehnen, P. R. Schreiner, *Organometallics* **2019**, *38*, 329–335.
- [12] N. W. Rosemann, J. P. Eußner, E. Dornsiepen, S. Chatterjee, S. Dehnen, *J. Am. Chem. Soc.* **2016**, *138*, 16224–16227.
- [13] N. Rinn, L. Guggolz, J. Lange, S. Chatterjee, T. Block, R. Pöttgen, S. Dehnen, *Chem. Eur. J.* **2018**, *24*, 5840–5848.
- [14] T. S. Basu Baul, A. Chaurasiya, A. Lyčka, I. Rojas-León, H. Höpfl, *J. Organomet. Chem.* **2019**, *898*, 120859.
- [15] L. Tian, H. Yang, X. Zheng, Z. Ni, D. Yan, L. Tu, J. Jiang, *Appl. Organomet. Chem.* **2009**, *23*, 24–31.
- [16] L. Tian, X. Liu, X. Zheng, Y. Sun, D. Yan, L. Tu, *Appl. Organomet. Chem.* **2011**, *25*, 298–304.
- [17] Q. Liu, H. Zhang, X. Zheng, W. Wang, L. Tian, *Appl. Organomet. Chem.* **2016**, *30*, 630–637.
- [18] L.-J. Tian, Y.-X. Sun, X.-L. Zheng, X.-J. Liu, Y. Yu, X.-L. Liu, B.-C. Qian, *Chin. J. Chem.* **2007**, *25*, 312–318.
- [19] J. A. Lara-Cerón, V. M. Jiménez-Pérez, A. A. Molina-Paredes, H. V. Rasika Dias, A. Chávez-Reyes, H. R. Paudel, M. E. Ochoa, B. M. Muñoz-Flores, *Eur. J. Inorg. Chem.* **2017**, 2818–2827.
- [20] N. Kobakhidze, N. Farfán, M. Romero, J. M. Méndez-Stivalet, M. G. Ballinas-López, H. García-Ortega, O. Domínguez, R. Santillan, F. Sánchez-Bar téz, I. Gracia-Mora, *J. Organomet. Chem.* **2010**, *695*, 1189–1199.
- [21] J. M. Rivera, H. Reyes, A. Cortes, R. Santillan, P. G. Lacroix, C. Lepetit, K. Nakatani, N. Farfan, *Chem. Mater.* **2006**, *18*, 1174–1183.
- [22] N. Singh, N. Srivastav, R. Singh, V. Kaur, E. Brendler, J. Wagler, E. Korke, *New J. Chem.* **2018**, *42*, 1655–1664.
- [23] N. Singh, K. Kumar, N. Srivastav, R. Singh, V. Kaur, J. P. Jasinski, R. J. Butcher, *New J. Chem.* **2018**, *42*, 8756–8764.
- [24] R. Vinayak, H. P. Nayek, *New J. Chem.* **2019**, *43*, 7259–7268.
- [25] M. D. Hartle, M. D. Pluth, *Chem. Soc. Rev.* **2016**, *45*, 6108–6117.
- [26] S. Fiorucci, E. Antonelli, A. Mencarelli, S. Orlandi, B. Renga, G. Rizzo, E. Distrutti, V. Shah, A. Morelli, *Hepatology* **2005**, *42*, 539–548.
- [27] M. D. Hammers, M. J. Taormina, M. M. Cerda, L. A. Montoya, D. T. Seidenkranz, R. Parthasarathy, M. D. Pluth, *J. Am. Chem. Soc.* **2015**, *137*, 10216–10223.
- [28] L. A. Montoya, M. D. Pluth, *Anal. Chem.* **2016**, *88*, 5769–5774.
- [29] L. Chen, D. Wu, C. S. Lim, D. Kim, S.-J. Nam, W. Lee, G. Kim, H. M. Kim, J. Yoon, *Chem. Commun.* **2017**, *53*, 4791–4794.
- [30] C. S. Park, T. H. Ha, S. Choi, D. N. Nguyen, S. Noh, O. S. Kwon, C. Lee, H. Yoon, *Biosens. Bioelectron.* **2017**, *89*, 919–926.
- [31] S. K. Patra, S. K. Sheet, B. Sen, K. Aguan, D. R. Roy, S. Khatua, *J. Org. Chem.* **2017**, *82*, 10234–10246.
- [32] J. Liu, X. Guo, R. Hu, X. Liu, S. Wang, S. Li, Y. Li, G. Yang, *Anal. Chem.* **2016**, *88*, 1052–1057.
- [33] M. L. Aulsebrook, S. Biswas, F. M. Leaver, M. R. Grace, B. Graham, A. M. Barrios, K. L. Tuck, *Chem. Commun.* **2017**, *53*, 4911–4914.
- [34] J. Holeček, M. Nádvořník, K. Handlíř, A. Lyčka, *J. Organomet. Chem.* **1986**, *315*, 299–308.
- [35] J. Holeček, A. Lyčka, M. Nádvořník, K. Handlíř, *Collect. Czech. Chem. Commun.* **1990**, *55*, 1193–1207.
- [36] J. Holeček, A. Lyčka, *Inorg. Chim. Acta* **1986**, *118*, L15–L16.
- [37] K. Sisido, T. Takeda, J. Kinigawa, *J. Am. Chem. Soc.* **1961**, *83*, 538–541.
- [38] A. D. Becke, *J. Chem. Phys.* **1993**, *98*, 5648–5652.
- [39] M. Cossi, V. Barone, *J. Chem. Phys.* **2001**, *115*, 4708–4717.
- [40] K. Sarma, T. S. Basu Baul, W. L. Basaiawmoit, R. Saran, *Spectrochim. Acta Part A* **1993**, *49*, 1027.
- [41] T. S. Basu Baul, P. Das, A. K. Chandra, S. Mitra, S. M. Pyke, *Dyes Pigment.* **2009**, *82*, 379–386.

Received: February 21, 2020